

Late sodium current in human, canine and guinea pig ventricular myocardium



Balázs Horváth^{a,b}, Tamás Hézsó^a, Norbert Szentandrassy^{a,c}, Kornél Kistamás^a, Tamás Árpádfy-Lovas^d, Richárd Varga^d, Péter Gazdag^d, Roland Veress^a, Csaba Dienes^a, Dóra Baranyai^a, János Almásy^a, László Virág^d, Norbert Nagy^d, István Baczkó^d, János Magyar^{a,e}, Tamás Bányász^a, András Varró^{d,f,*}, Péter P. Nánási^{a,g,**}

^a Department of Physiology, Faculty of Medicine, University of Debrecen, Debrecen, Hungary

^b Faculty of Pharmacy, University of Debrecen, Debrecen, Hungary

^c Department of Basic Medical Sciences, Faculty of Dentistry, University of Debrecen, Debrecen, Hungary

^d Department of Pharmacology and Pharmacotherapy, Faculty of Medicine, University of Szeged, Szeged, Hungary

^e Division of Sport Physiology, Department of Physiology, Faculty of Medicine, University of Debrecen, Debrecen, Hungary

^f Division of Cardiovascular Pharmacology, Hungarian Academy of Sciences, Szeged, Hungary

^g Department of Dental Physiology and Pharmacology, Faculty of Dentistry, University of Debrecen, Debrecen, Hungary

ARTICLE INFO

Keywords:

Late Na⁺ current
Ventricular repolarization
Action potential voltage clamp
Dog myocytes
Human myocytes

ABSTRACT

Although late sodium current ($I_{Na-late}$) has long been known to contribute to plateau formation of mammalian cardiac action potentials, lately it was considered as possible target for antiarrhythmic drugs. However, many aspects of this current are still poorly understood. The present work was designed to study the true profile of $I_{Na-late}$ in canine and guinea pig ventricular cells and compare them to $I_{Na-late}$ recorded in undiseased human hearts. $I_{Na-late}$ was defined as a tetrodotoxin-sensitive current, recorded under action potential voltage clamp conditions using either canonic- or self-action potentials as command signals. Under action potential voltage clamp conditions the amplitude of canine and human $I_{Na-late}$ monotonically decreased during the plateau (decrecendo-profile), in contrast to guinea pig, where its amplitude increased during the plateau (crescendo profile). The decrecendo-profile of canine $I_{Na-late}$ could not be converted to a crescendo-morphology by application of ramp-like command voltages or command action potentials recorded from guinea pig cells. Conventional voltage clamp experiments revealed that the crescendo $I_{Na-late}$ profile in guinea pig was due to the slower decay of $I_{Na-late}$ in this species. When action potentials were recorded from multicellular ventricular preparations with sharp microelectrode, action potentials were shortened by tetrodotoxin, which effect was the largest in human, while smaller in canine, and the smallest in guinea pig preparations. It is concluded that important interspecies differences exist in the behavior of $I_{Na-late}$. At present canine myocytes seem to represent the best model of human ventricular cells regarding the properties of $I_{Na-late}$. These results should be taken into account when pharmacological studies with $I_{Na-late}$ are interpreted and extrapolated to human. Accordingly, canine ventricular tissues or myocytes are suggested for pharmacological studies with $I_{Na-late}$ inhibitors or modifiers. Incorporation of present data to human action potential models may yield a better understanding of the role of $I_{Na-late}$ in action potential morphology, arrhythmogenesis, and intracellular calcium dynamics.

1. Introduction

Although late Na⁺ current ($I_{Na-late}$) is an important current flowing during the action potential (AP) plateau in mammalian cardiomyocytes

with physiological and pathological significance recognized long ago [1–3], its pathophysiological role in LQT3 [4] and heart failure [5–8] has been emphasized only in the last decades. $I_{Na-late}$ - as an inward current - contributes to plateau formation and is responsible for largely

Abbreviations: $I_{Na-late}$, late sodium current; AP, action potential; APD, action potential duration; APVC, action potential voltage clamp; TTX, tetrodotoxin; ATX-II, sea-anemone toxin

* Correspondence to: A. Varró, Department of Pharmacology and Pharmacotherapy, University of Szeged, H-6701 Szeged, Dóm tér 12, Hungary.

** Correspondence to: P.P. Nánási, Department of Physiology, University of Debrecen, H-4012 Debrecen, Nagyterdei krt 98, Hungary.

E-mail addresses: varro.andras@med.u-szeged.hu (A. Varró), nanasi.peter@med.unideb.hu (P.P. Nánási).

<https://doi.org/10.1016/j.yjmcc.2019.12.015>

Received 9 October 2019; Received in revised form 18 December 2019; Accepted 25 December 2019

Available online 17 January 2020

0022-2828/ © 2020 Elsevier Ltd. All rights reserved.

half of the transmembrane Na^+ entry [9–11]. As a consequence, the elevation of $I_{\text{Na-late}}$ results in increased arrhythmia propensity (e.g. in heart failure) including prolongation of the action potential duration (APD), increased inhomogeneity of repolarization and occurrence of early as well as delayed afterdepolarizations [5,12–14]. Therefore, as a new concept, intensive efforts were made recently to develop selective inhibitors of $I_{\text{Na-late}}$ [9,15,16].

Initially $I_{\text{Na-late}}$ was believed to be a consequence of the overlapping steady-state activation and inactivation functions of the Na^+ current (window Na^+ current) [17], now it is better explained by the slow inactivation kinetics of a small fraction of cardiac Na^+ channels (mode-II gating, bursting and late openings) [4,6]. In spite of its relative importance, many aspects of $I_{\text{Na-late}}$ are still poorly understood. In contrast to the detailed data obtained in rabbit [18], guinea pig [19] and porcine [20] myocytes, we have only a limited number of recordings of native human and canine $I_{\text{Na-late}}$, since these experiments were typically performed using conventional voltage clamp arrangements and many of them at room temperature [7,8,21–23]. Self action potential voltage clamp measurements, delivering the cell's own AP as a command signal, are not available in the literature either for canine or human ventricular cardiomyocytes. Since canine ventricular cells are believed to be a good model for human ventricular myocytes in general regarding their cellular electrophysiological properties [24–26], our goal was to monitor and compare the profiles of $I_{\text{Na-late}}$ in ventricular cells obtained from canine, guinea pig and undiseased human hearts. The rationale of our work is given by the very limited availability of undiseased human ventricular tissues for experimental purposes, and our results show that canine myocytes - but not guinea pig cells - are reasonably suitable preparations for studying the properties of human $I_{\text{Na-late}}$.

2. Methods

2.1. Preparations

Adult mongrel dogs of either sex (35 animals) were anesthetized with intramuscular injections of 10 mg/kg ketamine hydrochloride (Calypsol, Richter Gedeon, Hungary) + 1 mg/kg xylazine hydrochloride (Sedaxylan, Eurovet Animal Health BV, The Netherlands) according to a protocol approved by the local Animal Care Committee (license N^o: 9/2015/DEMÁB). All animal procedures conform to the guidelines from Directive 2010/63/EU of the European Parliament on the protection of animals used for scientific purposes. Bilateral palpebral reflex, jaw tone and response to bilateral painful stimuli (toe pinch) was assessed in every 2 min to monitor the depth of anesthesia. The surgical procedure started after the palpebral reflex and the withdrawal response to painful stimuli had been absent on both sides, there had been no immediate respiratory response to painful stimuli and there had been a considerable drop in the jaw tone for at least 6 min (three consecutive assessments).

Male guinea pigs (22 animals) were heparinized and anesthetized with nembutal (100 mg/kg i.p.). After achieving deep anesthesia the hearts were rapidly removed and mounted on a Langendorff apparatus allowing for retrograde perfusion of the aorta.

Undiseased human hearts ($n = 5$) were obtained from organ donors who did not receive medication except furosemide, dobutamine or plasma expanders. The valves were utilized for pulmonary and aortic valve transplantation surgery, and the remaining unused ventricular tissues were used for experimental purposes. After explantation, the hearts were stored in cardioplegic solution at 5 °C prior to dissection. The experimental protocols conform to the principles outlined in the Declaration of Helsinki and were approved by the University of Szeged and National Scientific and Research Ethical Review Boards (4991–0/2010-1018EKU, 339/PI/010).

Left ventricular trabeculae were dissected from the hearts and were used for recording of AP using sharp microelectrodes.

2.2. Isolation of cardiomyocytes

Single canine and human myocytes were obtained by enzymatic dispersion using the segment perfusion technique, as described previously [27]. Briefly, a wedge-shaped section of the ventricular wall supplied by the left anterior descending coronary artery was cannulated, dissected and perfused with a nominally Ca^{2+} -free Joklik solution (Minimum Essential Medium Eagle, Joklik Modification, Sigma-Aldrich Co. St. Louis, MO, USA) for 5 min. This was followed by 30 min long perfusion with Joklik solution supplemented with 1 mg/ml collagenase (Type II, Worthington Biochemical Co., Lakewood, NJ, USA; representing final activity of 224 U/ml) and 0.2% bovine serum albumin (Fraction V., Sigma) containing 50 μM Ca^{2+} . After this, normal external Ca^{2+} concentration was gradually restored and cells were stored in Minimum Essential Medium Eagle until use.

Guinea pig ventricular cells were obtained using a standard retrograde perfusion technique as previously described [19]. After mounting the aorta on a Langendorff device the heart was washed with oxygenized Tyrode solution for 5 min and further 3 min with Ca -free Tyrode solution to stop the heart. This superfusate was supplemented with 0.6 mg/ml collagenase (Type II, Worthington Biochemical Co., Lakewood, NJ, USA) and 0.05 mg/ml protease (Type XIV, Sigma-Aldrich Co., St. Louis, MO, USA). After this procedure the left ventricle was minced into tissue chunks which were further incubated with enzyme solution for approximately 1 h. After harvesting the cells the normal external Ca^{2+} concentration was restored.

2.3. Electrophysiology

Cells were placed in a 1 ml volume plexiglass chamber and continuously superfused with a modified Tyrode solution supplied by a gravity driven system at a speed of 1–2 ml/min. The modified Tyrode solution contained (in mM): NaCl 121, KCl 4, CaCl_2 1.3, MgCl_2 1, HEPES 10, NaHCO_3 25, glucose 10 at pH = 7.35. Osmolarity of the modified Tyrode solution was 300 ± 3 mOsm, measured with a vapor pressure osmometer (Vapro 5520, Wescor Inc., Logan, UT, USA). During experiments the bath temperature was set to 37 °C by a temperature controller (Cell MicroControls, Norfolk, VA, USA). The cells were visualized by an inverted microscope (Eclipse TE2000-U or Diaphot 300, Nikon, Japan) placed in a Faraday cage on an anti-vibration table. Electrical signals were recorded with intracellular amplifiers (MultiClamp 700A or 700B, Molecular Devices, Sunnyvale, CA, USA) and recorded with pClamp 10 software (Molecular Devices) after analogue-digital conversion (Digidata 1440A or 1332, Molecular Devices). Electrodes were fabricated from borosilicate glass having tip resistances of 2–3 M Ω after filling with pipette solution. Membrane currents were recorded using the whole-cell configuration of the patch-clamp technique. After establishing high (1–10 G Ω) resistance seal by gentle suction, the cell membrane beneath the tip of the electrode was disrupted by further suction or by applying 1.5 V electrical pulses for 1 ms. The series resistance was typically 4–8 M Ω . Experiments were discarded when the series resistance changed substantially during the measurement. The regular pipette solution contained (in mM): K-aspartate 120, KCl 30, MgATP 3, HEPES 10, Na_2 -phosphocreatine 3, EGTA 0.01, cAMP 0.002, KOH 10 at pH = 7.3. The osmolarity of the pipette solutions was 285 mOsm.

2.3.1. Action potential voltage clamp

Action potential voltage clamp (APVC) experiments were conducted according to the methods described previously [28–30]. Two types of APVC arrangements were applied. In the majority of experiments the cell's own AP was used as the command voltage (self APVC). In other experiments a previously recorded “canonic” midmyocardial action potential (possessing average parameters and configuration) was applied to the voltage clamped cells as command signal (canonic APVC). Current traces were recorded continuously under reference conditions

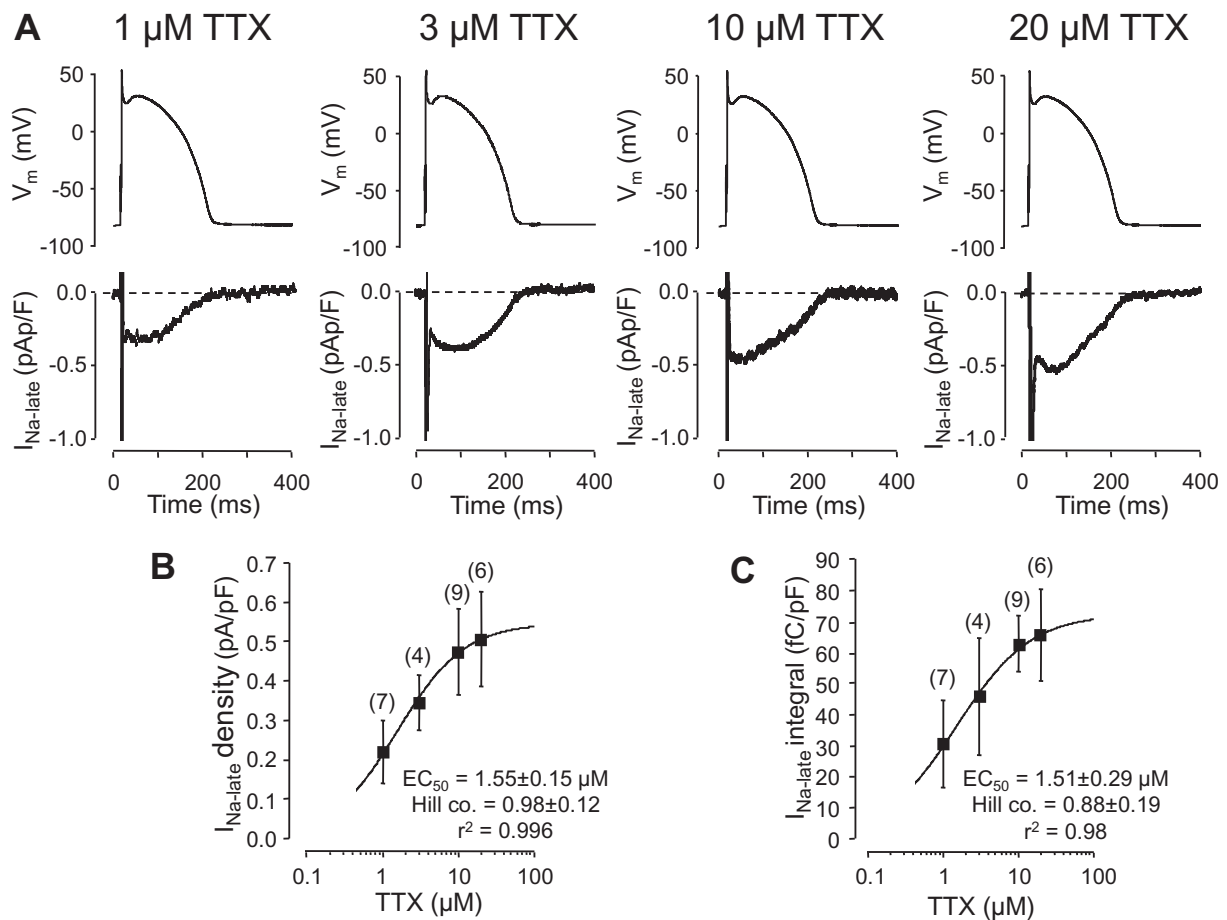


Fig. 1. Concentration-dependent effect of tetrodotoxin (TTX) in isolated canine ventricular myocytes under APVC conditions. For the sake of better comparability canonic APs were used as command signals (shown in the upper row). Furthermore, in order to exclude any contamination by L-type Ca^{2+} current, these experiments were performed in the presence of $1 \mu\text{M}$ nisoldipine. A: Representative records of $I_{\text{Na-late}}$ dissected by increasing concentrations of TTX. Exposure to TTX lasted for 5 min in each case. B and C: Concentration-response curves obtained for $I_{\text{Na-late}}$ measured 15 ms after the AP upstroke (B), and the net charge mediated by the current (C). The solid curve was obtained by fitting data to the Hill equation. Symbols and bars denote mean \pm SEM values, numbers in parentheses indicate the number of cells studied, derived from 5 animals.

(I_0), and after 5 min superfusion with the specific Na^+ channel inhibitor tetrodotoxin (I_{TTX}). $I_{\text{Na-late}}$ was defined as a TTX-sensitive current, obtained by subtracting the post-TTX traces from the reference traces ($I_{\text{Na-late}} = I_0 - I_{\text{TTX}}$). During the analysis of $I_{\text{Na-late}}$ the initial 15 ms after the AP upstroke (as indicated) was excluded from evaluation in order to omit the early Na^+ current peak. To account for trace-to-trace fluctuations and to reduce noise, 20 consecutive $I_{\text{Na-late}}$ traces were averaged, and the averaged curve was used for later analysis. $I_{\text{Na-late}}$ was usually normalized to cell capacitance, determined in each cell by applying hyperpolarizations from $+10$ to -10 mV for 15 ms.

2.3.2. Conventional voltage clamp

Conventional voltage clamp experiments, using rectangular command pulses, were performed with canine, human and guinea pig ventricular myocytes in order to study the density and inactivation characteristics of $I_{\text{Na-late}}$. In this case the external solution contained $1 \mu\text{M}$ nisoldipine to block L-type Ca^{2+} current and the rapid and slow delayed rectifier K^+ currents were blocked by application of $0.1 \mu\text{M}$ dofetilide and $0.5 \mu\text{M}$ HMR-1556, respectively. Test pulses were clamped to -20 mV from the holding potential of -120 mV before and after superfusion with $20 \mu\text{M}$ TTX, and $I_{\text{Na-late}}$ was considered as a result of the pharmacological subtraction. These $I_{\text{Na-late}}$ records (after exclusion of the initial 50 ms period) were fitted to a monoexponential function.

2.3.3. Recording of action potentials from multicellular preparations

Left ventricular trabeculae, dissected from canine, human and guinea pig ventricles, were used for AP recording. Multicellular preparations were selected to prevent the limitations inherent to single myocyte studies, like absence of intercellular clefts, potential damage to channel proteins *etc.*, allowing better simulation of *in vivo* conditions. Transmembrane potentials were recorded using 3M KCl filled sharp glass microelectrodes having tip resistance between 10 and $20 \text{M}\Omega$. These electrodes were connected to the input of a high impedance electrometer (MDE GmbH, Heidelberg, Germany). Preparations were paced through a pair of platinum electrodes using 1ms wide rectangular current pulses with twice threshold amplitude. The pacing cycle length was initially set to 1s for at least 60min allowing the preparations to equilibrate before starting the measurement. After taking recordings at this steady 1s cycle length, the pacing cycle length was sequentially varied between 0.3 and 5s . The 25th AP was measured at each cycle length, and the cycle length was then changed so that quasi-steady-state frequency-response relations could be obtained rapidly. APs were digitized at 100kHz using an ADA 3300 data acquisition board (Real Time Devices Inc., State College, PA, USA) and stored for later analysis. After taking control records at each cycle length the preparations were superfused with $2 \mu\text{M}$ TTX for 20min and the entire protocol was repeated in the presence of TTX. Efforts were made to maintain the same impalement throughout each experiment. If, however, an impalement became dislodged, adjustment was attempted, and

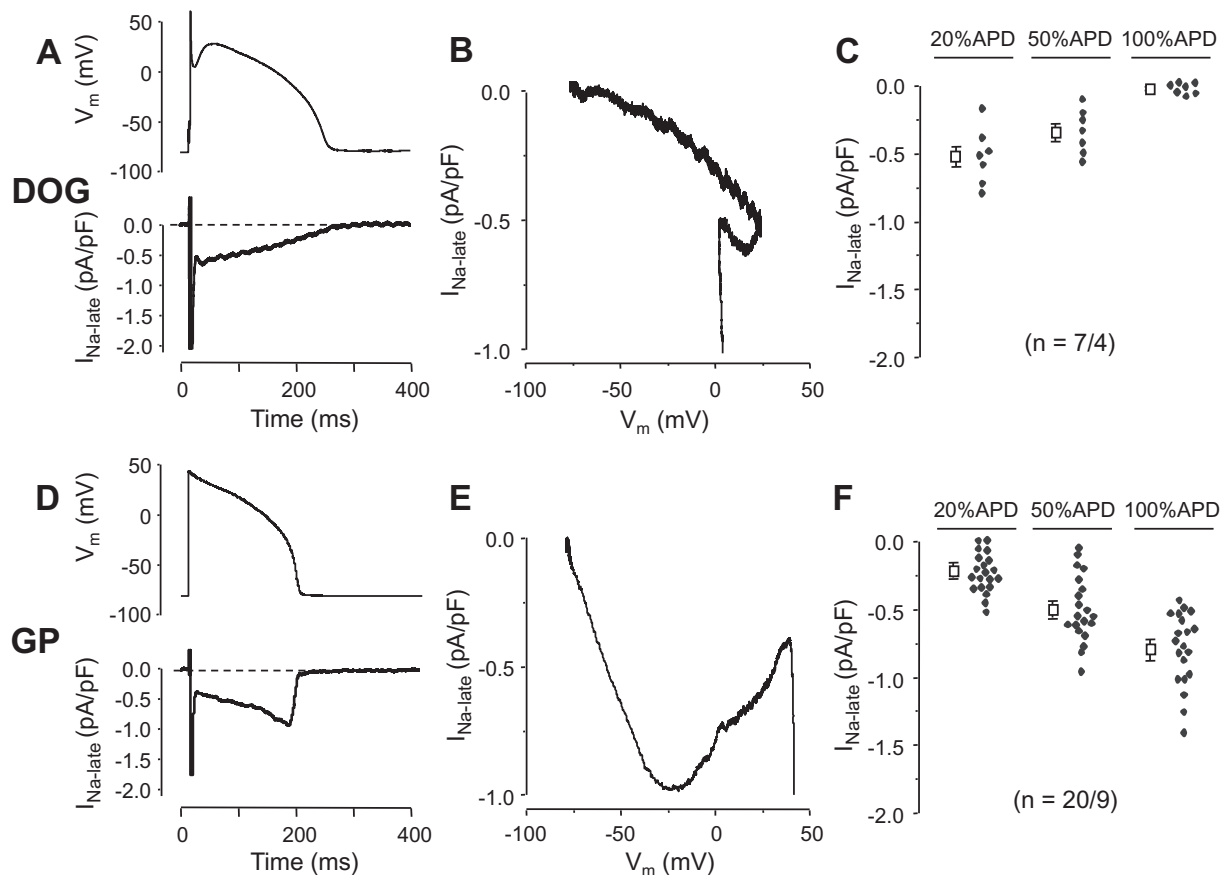


Fig. 2. True profiles of $I_{Na-late}$ recorded in canine (A–C) and guinea pig (D–F) ventricular cells under self APVC conditions. Currents were dissected by 10 μ M TTX. A, D: Representative records displaying $I_{Na-late}$ profiles (command APs above). B, E: Phase-plane trajectories obtained from the same records. C, F: Densities of $I_{Na-late}$ measured at 20%, 50% and 100% of APD, where APD_{90} was defined as 100%. Symbols and bars are mean \pm SEM values, blue dots represent individual data, numbers in parentheses indicate the number of myocytes/number of animals studied.

if the characteristics of the re-established impalement deviated by < 5% from the previous measurement, the experiment continued.

2.4. Statistics

Results are expressed as mean \pm SEM values, the number of myocytes or multicellular preparations studied/derived from the number of animals is given in parenthesis. In the graphs individual data are denoted by blue dots. Statistical significance of differences was evaluated using one-way ANOVA followed by Student's *t*-test. Differences were considered significant when p was < 0.05.

Chemicals used in the experiments were obtained from Sigma-Aldrich Co. (St. Louis, MO, USA).

3. Results

Primarily the optimal TTX concentration for dissection $I_{Na-late}$ in canine ventricular myocytes had to be determined in order to find a TTX concentration that is suitable to excise a sufficiently large portion of $I_{Na-late}$ allowing visualization of the true profile of the current. Representative records presented in Fig. 1.A indicate that the effect of TTX tends to saturate at the concentration of 10 μ M. Based on the concentration-response curves obtained by fitting these data to the Hill equation (Fig. 1.B, C) 10 μ M TTX caused an approximately 87% inhibition of the current. Therefore 10 μ M TTX was chosen to dissect $I_{Na-late}$ in the forthcoming voltage clamp experiments bearing in mind that this approach is likely to somewhat underestimate the density and integral of $I_{Na-late}$. Accordingly, the relative contribution of the high TTX-

affinity “neuronal” Na^+ channels were not monitored, *i.e.* the effects of lower (nanomolar) TTX concentrations were not studied. This may distort somewhat the EC_{50} values obtained for TTX in Fig. 1.B and C. These measurements were performed in the presence of 1 μ M nisoldipine to suppress L-type Ca^{2+} current, since large concentrations of TTX have been shown to inhibit Ca^{2+} current as well [31,32].

As has been shown in Fig. 1 (canonic APVC in nisoldipine) and Fig. 2.A (self APVC without nisoldipine), canine $I_{Na-late}$ displayed a “decrescendo” profile, *i.e.* its amplitude decreased monotonically during the time course of the AP, in contrast to guinea pig ventricular myocytes, where the amplitude of the current was increasing during the plateau and declined only on terminal repolarization (Fig. 2.D, “crescendo profile”). These differences are also reflected by the current-voltage relations (phase-plane trajectories) obtained under the APs in canine and guinea pig cells (Fig. 2.B and E). More quantitative approach to demonstrate the profile of $I_{Na-late}$ is to measure the density of the TTX-sensitive current at 20%, 50% and 100% of APD, where the APD at 90% repolarization (APD_{90}) was considered as 100% (Fig. 2.C and F). Accordingly, the density of $I_{Na-late}$ at 20% APD was -0.52 ± 0.09 pA/pF in dog versus the -0.21 ± 0.05 pA/pF in guinea pig ($p < .05$), while at 100% APD $I_{Na-late}$ had a greater density in guinea pig than dog (-0.78 ± 0.07 versus -0.03 ± 0.02 pA/pF, $p < .05$). At 50% APD the densities were not significantly different in the two species. Although the charge carried by $I_{Na-late}$ was higher in guinea pig than in dog (86.2 ± 10.8 fC/pF, $n = 20/9$ versus 67.1 ± 9.2 fC/pF, $n = 7/4$, $p < .05$) these current integrals were in a similar range.

As already mentioned above, $I_{Na-late}$ current profiles in canine

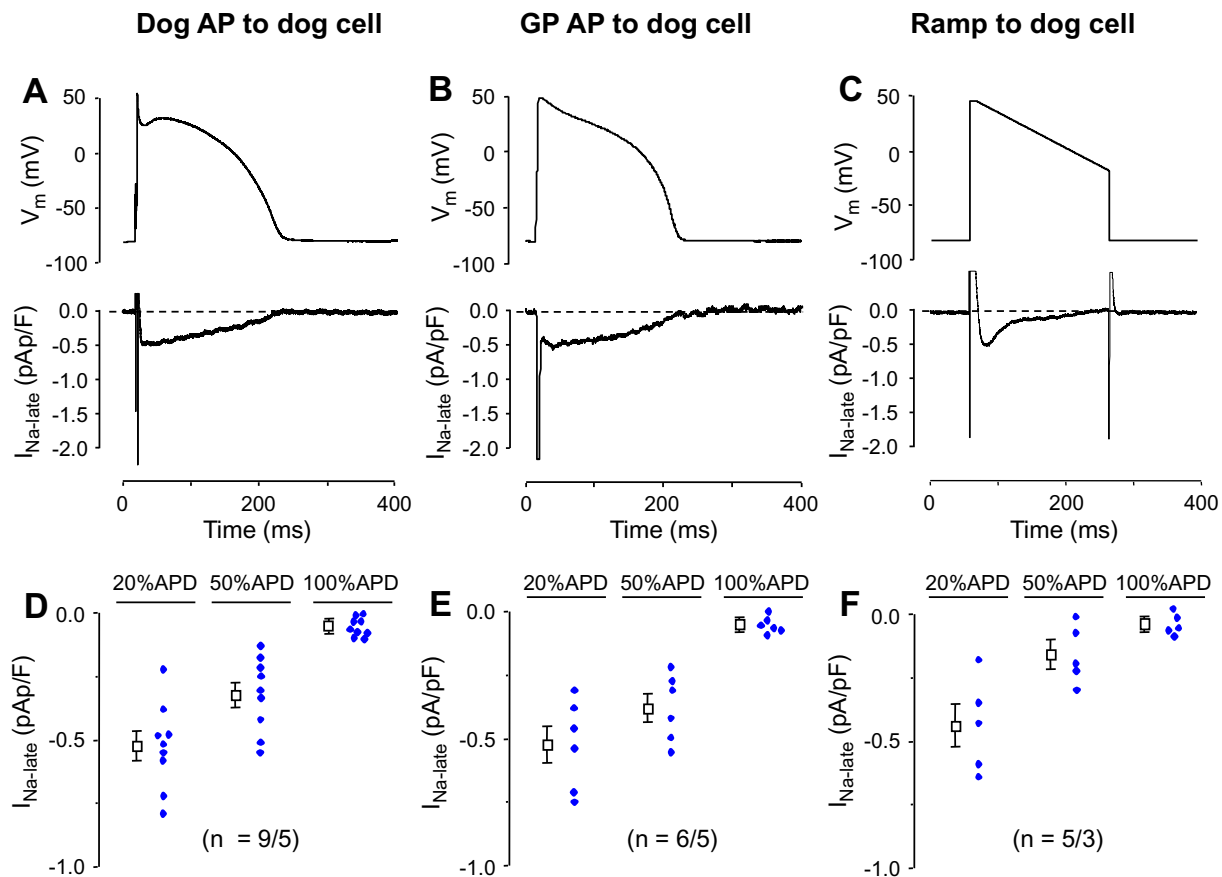


Fig. 3. Effect of the shape of command voltage on the profile of $I_{Na-late}$ in canine myocytes.

A-C: Representative sets of records displaying command voltage protocols (upper row) and the recorded $I_{Na-late}$ profiles dissected by $10\ \mu\text{M}$ TTX in the presence of $1\ \mu\text{M}$ nisoldipine (lower row). A canonic dog AP was delivered to a canine cell in panel A, in B a canonic guinea pig AP was applied to a canine cell, while in C a decaying voltage ramp was used as a command signal. D-F: $I_{Na-late}$ densities measured at 20%, 50% and 100% of APD (100% = APD_{90}) under conditions shown in panels A-C. Symbols and bars are mean \pm SEM values, blue dots represent individual data, numbers in parentheses indicate the number of myocytes/number of animals studied.

cardiomyocytes were determined under APVC conditions in two slightly different experimental groups. In the first group canonic APVC was used and $I_{Na-late}$ was determined in the presence of $1\ \mu\text{M}$ nisoldipine (Fig. 1, $n = 9/5$). In the second group self APVC was used without nisoldipine (Fig. 2.A-C, $n = 7$). Although the values were somewhat smaller in the presence of nisoldipine, no significant differences were found between the two groups at 20%, 50% or 100% APD (-0.48 ± 0.08 versus -0.52 ± 0.09 pA/pF, -0.30 ± 0.06 versus -0.34 ± 0.06 pA/pF and -0.06 ± 0.02 versus -0.03 ± 0.02 pA/pF, respectively). The integrals were also similar (63.1 ± 9.2 fC/pF, $n = 9/5$ versus 67.1 ± 9.2 fC/pF, $n = 7/4$, respectively, N.S.). This comparison suggests that $10\ \mu\text{M}$ concentration of TTX does not interfere with the L-type Ca^{2+} current.

Since AP configuration has been shown to influence current profiles under APVC conditions [28,29], attempts were made to convert the decrescendo type canine $I_{Na-late}$ into a crescendo profile, characteristic of guinea pig myocytes. Therefore, duration-matched canonic guinea pig APs (Fig. 3.B,E) and voltage ramps resembling the ramp-like plateau of guinea pig cells (Fig. 3.C,F) were applied as command signals to canine cells. The ramp started from -80 mV, spent 10 ms at $+40$ mV and decayed to -20 mV during 200 ms. None of these interventions were capable to convert the canine decrescendo current profile to a crescendo guinea pig-like $I_{Na-late}$ profile. The current integrals were also similar in canine cells independently of the canine or guinea pig origin of the command AP (63.1 ± 9.2 fC/pF, $n = 9/5$ versus 65.4 ± 10.7 fC/pF, $n = 6/5$, N.S.).

The sea-anemone toxin (ATX-II) has been shown to induce a current

in cardiac tissues resembling $I_{Na-late}$ by removing the fast inactivation machinery of Na^+ channels [33]. In guinea pig myocytes the profile of the TTX-sensitive current was similar in the absence and presence of $10\ \text{nM}$ ATX-II (Fig. 4.A), although its amplitude was significantly increased by ATX-II (compare also Figs. 4.D and 2.F), i.e. the current followed crescendo kinetics in both cases. In contrast, canine myocytes usually produced early afterdepolarizations when exposed to $10\ \text{nM}$ ATX-II for 3 min (not shown), therefore the canine cells were treated with a lower, $1\ \text{nM}$ concentration of ATX-II. The TTX-sensitive current in these canine cells displayed a plateau-like shape, i.e. the current densities were largely similar at 20%, 50% and 100% APD in the presence of ATX-II (Fig. 4.B,E). This current profile, containing the sum of baseline $I_{Na-late}$ plus the ATX-II-induced current component, was markedly different from that recorded in the absence of ATX-II (compare Figs. 4.E and 2.C). Therefore, in another series of experiments, where the ATX-II-induced current alone was visualized, the ATX-II-induced current showed moderate crescendo characteristics in canine myocytes (Fig. 4.C,F). The TTX-sensitive current integrals were significantly larger in the presence of ATX-II ($1\ \text{nM}$ in canine and $10\ \text{nM}$ in guinea pig cells) comparing to untreated cells: 102 ± 13 fC/pF, $n = 7/4$ versus 67 ± 9 fC/pF, $n = 7/4$ in canine; and 145 ± 19 fC/pF, $n = 5/3$ versus 86 ± 11 fC/pF, $n = 20/9$ in guinea pig myocytes, $p < .05$ for both. The duration of action potentials (APD_{90}) was significantly increased by $1\ \text{nM}$ ATX-II in canine cells from 214 ± 13 ms to 257 ± 17 ms (lengthening of 43.2 ms, $n = 7/4$, $p < .05$), in contrast to guinea pig myocytes, where the increase induced by $10\ \text{nM}$ ATX-II (from 192 ± 15 to 212 ± 20 ms, lengthening of 19.5 ms, $n = 5/3$),

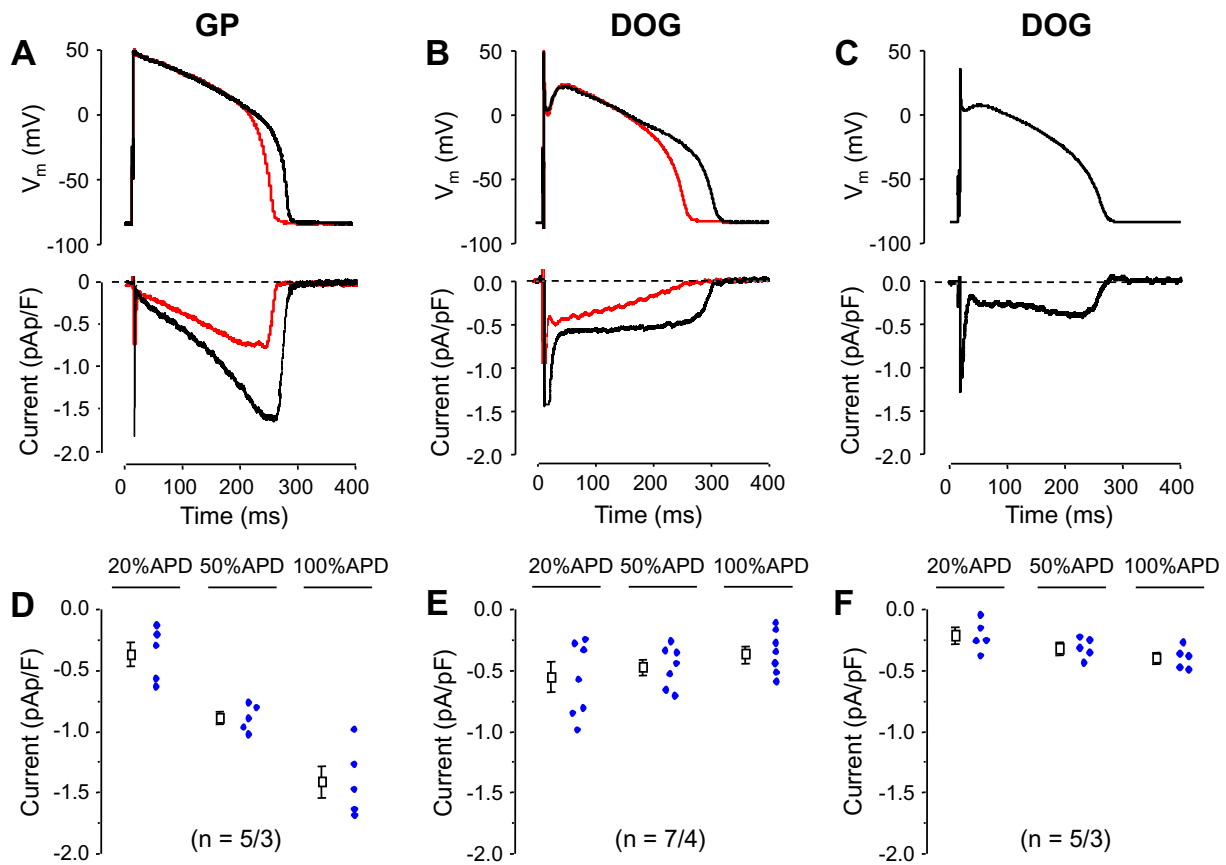


Fig. 4. Effect of ATX-II on the TTX-sensitive current profile in guinea pig and canine ventricular cells. In guinea pig myocytes (A, D) the TTX-sensitive current profile was similarly shaped (crescendo) in the absence (red records) or presence (black records) of 10 nM ATX-II, while in canine cells (B, E) the current profile was modified by 1 nM ATX-II. The control TTX-sensitive current records (red) are derived from different cells and presented exclusively for the sake of better comparison. The profile of the ATX-II-induced current in canine cells is displayed in panels C and F. Bottom panels display Na^+ current densities measured in the presence of ATX-II (D, E) and absence of ATX-II (F) at 20%, 50% and 100% of APD, where 100% = APD_{90} . Symbols and bars are mean \pm SEM values, blue dots represent individual data, numbers in parentheses indicate the number of myocytes/number of animals studied.

was not significant statistically. These results clearly demonstrate that canine myocytes are much more sensitive to ATX-II than the guinea pig cells, and more importantly, the profile of the ATX-II-induced current is different from the native $I_{\text{Na-late}}$ in canine myocytes.

In the following, the profiles (under self APVC conditions) and the kinetic properties (using conventional voltage clamp techniques) of $I_{\text{Na-late}}$ were compared in human, canine and guinea pig ventricular cells (Fig. 5). The 20 μM TTX-sensitive currents were similarly shaped in all types of myocytes when the membrane potential was switched from the holding potential of -120 mV to the test potential of -20 mV in the presence of 1 μM nisoldipine (Fig. 5.A-C). When the decay of TTX-sensitive current was fitted to a monoexponential function (excluding the initial 50 ms period) the inactivation time constants were 60 ± 3 ms ($n = 13/7$) in canine, 67 ± 5 ms ($n = 5/3$) in human, and 155 ± 16 ms ($n = 5/3$) in guinea pig cells. Thus the time course of inactivation of $I_{\text{Na-late}}$ was similar in human and canine myocytes, but was significantly ($p < .05$) slower in guinea pig. The corresponding current densities (obtained also by the monoexponential fitting procedure) were -0.47 ± 0.05 pA/pF in human, -0.56 ± 0.04 pA/pF in canine and -0.54 ± 0.14 pA/pF in guinea pig myocytes, which values were not significantly different. Representative $I_{\text{Na-late}}$ profiles recorded from a human, canine and guinea pig myocyte under self APVC conditions are presented in Fig. 5.D-F. These current profiles were also very similar in canine and human cells (both sharing the decrescendo $I_{\text{Na-late}}$ profile), while markedly different from the crescendo type $I_{\text{Na-late}}$ in guinea pig.

The rate-dependent effects of TTX on AP morphology in

multicellular ventricular preparations, obtained from the three species, is demonstrated in Fig. 6. All preparations were superfused with 2 μM TTX and the measurements were performed after equilibration. APD was shortened by TTX at each cycle length. The TTX-induced shortening, recorded at the cycle length of 1 s, was the largest (67 ± 16 ms, $n = 4/3$) in human, intermediate (21 ± 4 ms, $n = 5/5$) in canine and the smallest (11 ± 3 , $n = 7/7$) in guinea pig preparations. The resting membrane potential and the amplitude of AP were not altered by TTX. The maximum velocity of depolarization (dV/dt_{max}) was moderately reduced by TTX from 310 ± 48 to 259 ± 24 V/s in human, from 231 ± 40 to 169 ± 33 V/s in canine, and from 226 ± 32 to 176 ± 21 V/s in guinea pig, however, these changes failed to reach the level of significance – except for the canine preparations.

4. Discussion and conclusions

This is the first study to demonstrate the profiles of human and canine ventricular $I_{\text{Na-late}}$ under self APVC conditions. From this perspective our results are in line with those of Murphy et al. [23] who have shown the profile of canine $I_{\text{Na-late}}$ using canonic APs. Regarding undiseased human ventricular cells, this is the first report using the APVC technique. Our most important finding was to demonstrate that canine myocytes can be used as a reasonably good model to study human $I_{\text{Na-late}}$ - in contrast to myocytes originating from other mammals including guinea pigs, rabbits and pigs, since all in these latter species the current displays a crescendo profile [18–20]. Important implication of this interspecies difference is that the relative contribution of $I_{\text{Na-late}}$

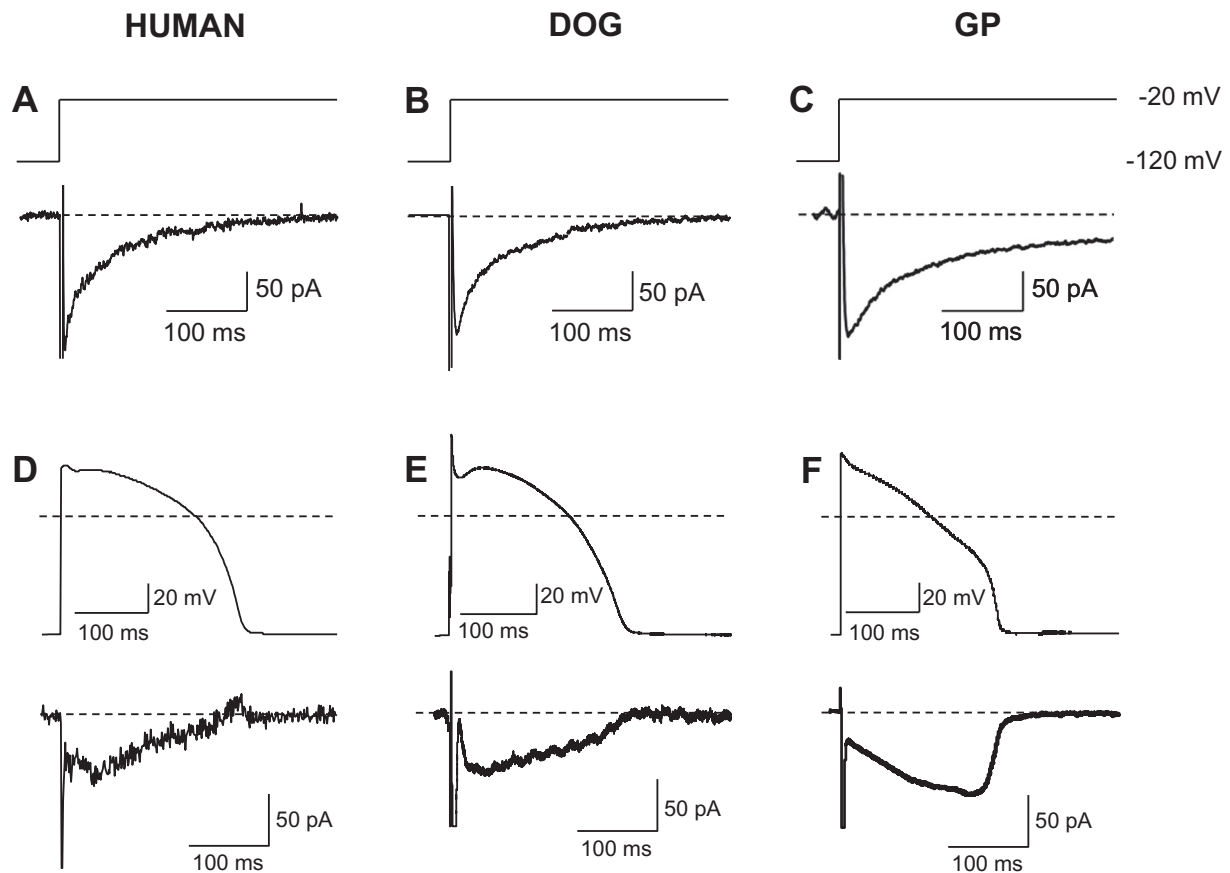


Fig. 5. Comparison the properties of $I_{Na-late}$ recorded from myocytes digested from human (A,D), canine (B,E) and guinea pig (C,F) ventricular myocardium. In panels A-C the 20 μ M TTX-sensitive currents were activated with rectangular voltage pulses clamped to -20 mV from the holding potential of -120 mV in the presence of 1 μ M nisoldipine, 0.1 μ M dofetilide and 0.5 μ M HMR-1556, while in D-F TTX was used to dissect $I_{Na-late}$ under self APVC conditions (without nisoldipine, dofetilide and HMR-1556).

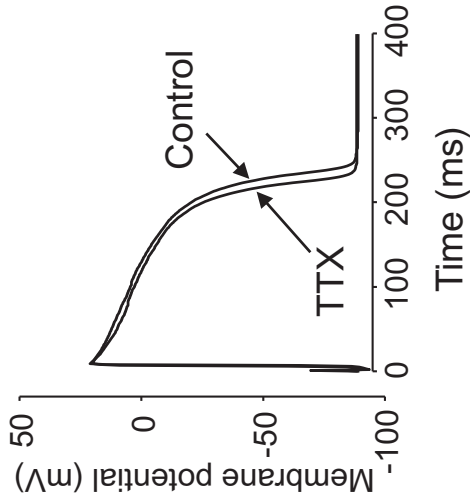
to action potential morphology (with the concomitant Na^+ and Ca^{2+} load resulting in increased arrhythmia propensity) increases with lengthening of APD in the “crescendo” group in contrast to the “de-crescendo” situation, and *vice versa*, it will be relatively smaller at shorter APDs. More explicitly, $I_{Na-late}$ is the largest in amplitude at the time of terminal repolarization in the “crescendo” type species, consequently, a given prolongation of APD (eg. due to application of a HERG channel inhibitor) is expected to cause a greater extra inward $I_{Na-late}$ current (together with larger Na^+ and Ca^{2+} load), which in turn, may magnify the APD lengthening effect of the K^+ channel inhibitor. Since $I_{Na-late}$ is practically inactivated at this time in the “de-crescendo” type preparations, changes in APD will barely modify the magnitude of Na^+ entry via $I_{Na-late}$. Using similar argumentation, the therapeutic effects of $I_{Na-late}$ inhibitors (including the shortening of APD and reduction of cellular Na^+ and Ca^{2+} content) is expected to be less pronounced in canine and human myocardium than in similar preparations from guinea pigs, rabbits and pigs. This should be taken into account when the results of pharmacological studies on $I_{Na-late}$ inhibitors or modifiers are interpreted or extrapolated to human, since some studies with such compounds have been performed in species displaying crescendo $I_{Na-late}$ profiles [34–36]. Based on the present results, canine ventricular tissues or myocytes are suggested for pharmacological studies with drugs interacting with $I_{Na-late}$.

We have also revealed why the guinea pig $I_{Na-late}$ is growing under the AP plateau, while canine and human $I_{Na-late}$ decreases during the time course of the AP. In canine and human myocytes the inactivation time constant of $I_{Na-late}$ was in the range of 60–67 ms at -20 mV, consequently the current became practically fully inactivated by the time of terminal repolarization. In contrast, the decay time constant

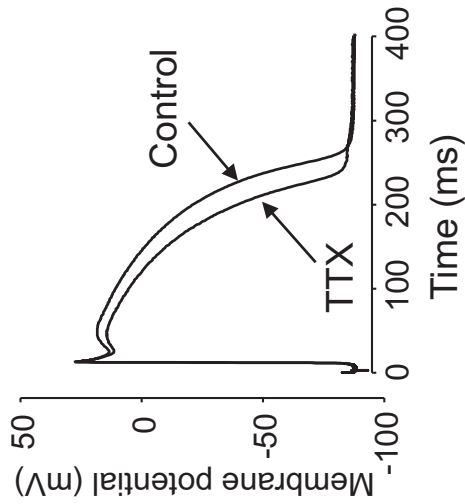
was much longer (156 ms) in guinea pig, thus the inactivation was slow enough to leave a significant portion of Na^+ channels open by the time of terminal repolarization. Consequently, the increasing inward driving force acting on Na^+ ions could increase the amplitude of $I_{Na-late}$ during the monotonic slow repolarization in guinea pig (and likely also in rabbit and pig). The well-known crescendo $I_{Na-late}$ profile in guinea pig was originally explained with the non-equilibrium gating theory of Clancy et al. [37]. This model predicts the accumulation of $I_{Na-late}$ during the plateau as a consequence of the ramp-like configuration of phase-2 repolarization of the guinea pig AP. However, application of guinea pig APs as well as repolarizing ramps as command signals failed to convert the decrescendo $I_{Na-late}$ profile of canine cells to crescendo, indicating that it is not the AP configuration, but rather the 2.5-fold slower inactivation kinetics, revealed by the conventional voltage clamp experiments, that accounts for the crescendo $I_{Na-late}$ profile in guinea pig. Since a portion of $I_{Na-late}$ is attributed to the function of non-cardiac Na^+ channels in the canine heart [38], it is possible that the type or relative contribution of these TTX-sensitive channels or variances in their regulatory subunits are different in dogs (and humans) versus guinea pigs (and pigs or rabbits). However, elucidating the details behind the different inactivation kinetics of $I_{Na-late}$ among various species warrants further studies.

Here is to be mentioned that there is a wide variety of SCN5 mutations, responsible for LQT3 syndrome, and depending on the site and type of mutation many parameters of Na^+ channel gating, including the rate of inactivation and recovery as well as the voltage dependence of activation and inactivation, may be altered, however, augmentation of $I_{Na-late}$ is a critical and common feature in all cases [39]. Since only a very small fraction of the total Na^+ channel population may contribute

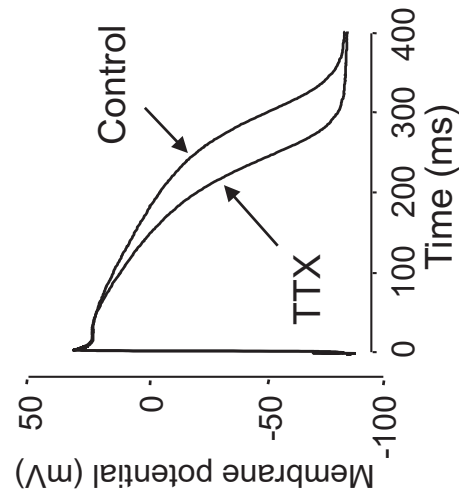
GP



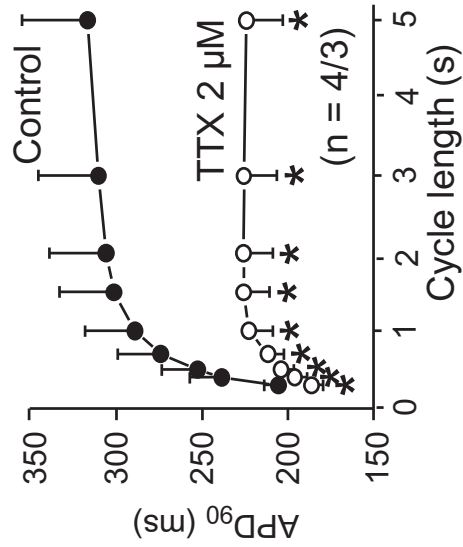
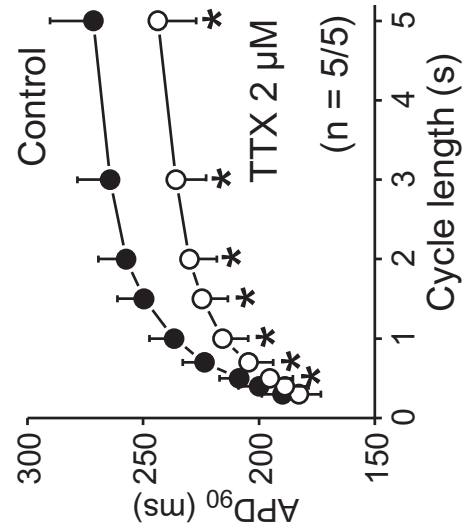
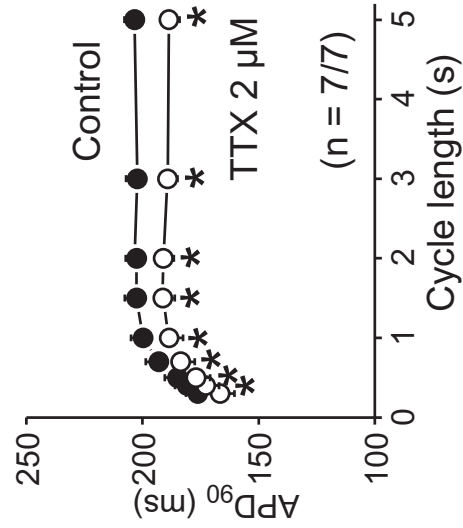
DOG



HUMAN



A



B

Fig. 6. Effects of 2 μM TTX on APD in multicellular human, canine and guinea pig ventricular preparations. These experiments were performed in a rate-dependent manner, where the cycle length was gradually changed between 0.3 and 5 s. Representative pairs of APs, recorded at cycle lengths of 1 s are depicted in the upper rows (A). B: Cycle length-dependent shortening effect of 2 μM TTX on APD. Symbols and bars represent mean \pm SEM values, asterisks indicate statistically significant differences between control and TTX data determined using one-way ANOVA followed by Student's t-test for paired data. Differences were considered significant when p was < 0.05 . The numbers in parentheses denote the number of preparations/number of animals studied.

to generation of $I_{Na-late}$ (compare the few tens of pA amplitude of $I_{Na-late}$ with the several nA amplitude of the peak Na^+ current), the macroscopic changes in I_{Na} gating are less relevant from the pathophysiological point of view than the actual magnitude of $I_{Na-late}$.

Another important result of the present study was to show that the profile of the ATX-II-induced current recorded under APVC conditions in canine cells is markedly different from the shape of native canine $I_{Na-late}$, since the ATX-II-induced current displayed a crescendo profile in both species – similar to the native $I_{Na-late}$ of guinea pig, rabbit and porcine hearts, but different from the native $I_{Na-late}$ recorded from canine myocytes. This may be related to the well-known fact that ATX-II slows inactivation of Na^+ channels [33]. ATX-II is widely used for mimicking pharmacologically the consequences of an augmented $I_{Na-late}$, which is often seen under pathological conditions [5] and ATX-II is a widely used pharmacological tool to model this. In canine myocytes (*i.e.* in the cells appearing to be the best model for studying human $I_{Na-late}$), however, this approach may be misleading due to the differences observed between the native $I_{Na-late}$ and ATX-II-induced current profiles. As a consequence, ATX-II modified Na^+ channels might also differ from the native channels in their in drug-sensitivity, making results obtained in the presence of ATX-II difficult to interpret.

APDs recorded from multicellular canine, human and guinea pig preparations were shortened by 2 μ M TTX, which effect was the largest in human, intermediate in canine and the smallest in guinea pig preparations. This sequence can not be explained by the known (and presently described) properties of $I_{Na-late}$, since the current densities and integrals were largely similar in the three species. It is more likely therefore that the magnitude of the TTX-induced shortening depends on the actual repolarization reserve of the myocardium [40,41], which is the smallest in human, intermediate in canine, and with the strong I_{Ks} is the largest in guinea pig ventricular myocardium [42,43]. This is a further argument in support of using canine myocytes for modeling human $I_{Na-late}$. This interspecies difference (*i.e.* dog vs. guinea pig) in repolarization reserve may explain also the higher ATX-II-sensitivity of dog comparing to guinea pig. In canine myocytes 1 nM ATX-II caused twice greater lengthening of AP than 10 nM ATX-II in guinea pig, while 10 nM ATX-II initiated early afterdepolarizations in canine cells.

In summary, we conclude that canine myocytes represent a reasonably suitable model of human ventricular cells regarding the properties of $I_{Na-late}$. However, further detailed studies are required to describe the gating kinetics of $I_{Na-late}$.

Funding

This work was funded by the National Research Development and Innovation Office (NKFIH-K115397 to P.P.N., NKFIH-PD120794 and NKFIH-FK128116 to B.H., NKFIH-PD125402 and NKFIH-FK129117 to N.N., and NKFIH-K119992 to A.V.). Further support was obtained from the GINOP-2.3.2.-15-2016-00040 and EFOP-3.6.2-16-2017-00006 projects, which are co-financed by the European Union and the European Regional Development Fund. The work was also supported by the Hungarian Academy of Sciences (János Bolyai Research Scholarship to B.H. and N.N.), and by the ÚNKP-19-4 and ÚNKP-19-2 New National Excellence Program of the Ministry of Human Capacities (to B.H., D.B.).

Declaration of Competing Interest

None declared.

References

- 1 E. Coraboeuf, E. Deroubaix, A. Coulombe, Effect of tetrodotoxin on action potentials of the conducting system in the dog heart, *Am. J. Phys.* 236 (1979) H561–H567.
- 2 E. Carmeliet, Slow inactivation of sodium current and voltage-dependent block by tetrodotoxin in rabbit cardiac Purkinje fibers, *Biomed. Biochim. Acta* 45 (1986) S163–S166.
- 3 E. Carmeliet, Voltage-dependent block by tetrodotoxin of the sodium channel in rabbit cardiac Purkinje fibers, *Biophys. J.* 51 (1987) 109–114.
- 4 K.R. Chadda, K. Jeevaratnam, M. Lei, C.L.H. Huang, Sodium channel biophysics, late sodium current and genetic arrhythmic syndromes, *Pflügers Arch.* 469 (2017) 629–641.
- 5 B. Horvath, D.M. Bers, The late sodium current in heart failure: pathophysiology and clinical relevance, *ESC Heart Failure* 1 (2014) 26–40.
- 6 A.I. Undrovinas, V.A. Maltsev, J.W. Kyle, N. Silverman, H.N. Sabbah, Gating of the late Na^+ channel in normal and failing human myocardium, *J. Mol. Cell. Cardiol.* 34 (2002) 1477–1489.
- 7 C.R. Valdivia, W.W. Chu, J. Pu, J.D. Foell, R.A. Haworth, Wolff MR et al. increased late sodium current in myocytes from a canine heart failure model and from failing human heart, *J. Mol. Cell. Cardiol.* 38 (2005) 475–483.
- 8 V.A. Maltsev, N. Silverman, H.N. Sabbah, A.I. Undrovinas, Chronic heart failure slows late sodium current in human and canine ventricular myocytes: implications for repolarization variability, *Eur. J. Heart Fail.* 9 (2007) 219–227.
- 9 Y. Song, L. Belardinelli, Basal late sodium current is a significant contributor to the duration of action potential of guinea pig ventricular myocytes, *Physiol. Rep.* (2017) e13295.
- 10 V.A. Maltsev, A.I. Undrovinas, A multi-modal composition of the late Na^+ current in human ventricular cardiomyocytes, *Cardiovasc. Res.* 69 (2006) 116–127.
- 11 D. Noble, P.J. Noble, Late sodium current in the pathophysiology of cardiovascular disease: consequences of sodium-calcium overload, *Heart* 92 (Suppl. 4) (2006) 1–5.
- 12 A. Zaza, M. Rocchetti, The late Na^+ current - origin and pathophysiological relevance, *Cardiovasc. Drugs Ther.* 27 (2013) 61–68.
- 13 J.C. Shyrook, Y. Song, S. Rajamani, C. Antzelevitch, L. Belardinelli, The antiarrhythmic consequences of increasing late I_{Na} in the cardiomyocyte, *Cardiovasc. Res.* 99 (2013) 600–611.
- 14 S. Yu, G. Li, C.L.H. Huang, M. Lei, L. Wu, Late sodium current associated cardiac electrophysiological and mechanical dysfunction, *Pflügers Arch.* 470 (2018) 461–469.
- 15 C. Antzelevitch, L. Belardinelli, The role of sodium channel current in modulating transmural dispersion of repolarization and arrhythmogenesis, *J. Cardiovasc. Electrophysiol.* 17 (Suppl. 1) (2006) S79–S85.
- 16 A.I. Undrovinas, L. Belardinelli, N.A. Undrovinas, H.N. Sabbah, Ranolazine improves abnormal repolarization and contraction in left ventricular myocytes of dogs with heart failure by inhibiting late sodium current, *J. Cardiovasc. Electrophysiol.* 17 (Suppl. 1) (2006) S169–S177.
- 17 D. Attwell, L.S. Cohen, D.A. Eisner, M. Ohba, C. Ojeda, The steady state TTX-sensitive (“window”) sodium current in cardiac Purkinje fibres, *Pflügers Arch.* 379 (1979) 137–142.
- 18 B. Hegyi, T. Bányász, L.T. Izu, L. Belardinelli, D.M. Bers, Y. Chen-Izu, β -Adrenergic regulation of late Na^+ current during cardiac action potential is mediated by both PKA and CaMKII, *J. Mol. Cell. Cardiol.* 123 (2018) 168–179.
- 19 B. Horvath, T. Banyasz, Z. Jian, B. Hegyi, K. Kistamas, P.P. Nanasi, et al., Dynamics of the late Na^+ current during cardiac action potential and its contribution to afterdepolarizations, *J. Mol. Cell. Cardiol.* 64 (2013) 59–68.
- 20 B. Hegyi, J. Bossuyt, L.G. Griffiths, R. Shimkunas, Z. Coulbaly, Z. Jian, et al., Complex electrophysiological remodeling in postinfarction ischemic heart failure, *Proc. Natl. Acad. Sci. U. S. A.* 115 (2018) E3036–E3044.
- 21 V.A. Maltsev, H.N. Sabbah, R.S.D. Higgins, N. Silverman, M. Lesch, A.I. Undrovinas, Novel, ultraslow inactivating sodium current in human ventricular cardiomyocytes, *Circulation* 98 (1998) 2545–2552.
- 22 A.C. Zygmunt, G.T. Eddelstone, G.P. Thomas, V.V. Nesterenko, C. Antzelevitch, Larger late sodium conductance in M cells contributes to electrical heterogeneity in canine ventricle, *Am. J. Physiol. Heart Circ. Physiol.* 281 (2001) H689–H697.
- 23 L. Murphy, D. Renodin, C. Antzelevitch, J.M. Di Diego, J.M. Cordeiro, Extracellular proton depression of peak and late Na^+ current in the canine left ventricle, *Am. J. Physiol. Heart Circ. Physiol.* 301 (2011) H936–H944.
- 24 G. Szabo, N. Szentandrassy, T. Biro, B.I. Toth, G. Czifra, J. Magyar, et al., Asymmetrical distribution of ion channels in canine and human left-ventricular wall: epicardium versus midmyocardium, *Pflügers Arch.* 450 (2005) 307–316.
- 25 N. Szentandrassy, T. Biro, G. Szabo, B.I. Toth, J. Magyar, et al., Apical-basal inhomogeneity in distribution of ion channels in canine and human ventricular myocardium, *Cardiovasc. Res.* 65 (2005) 851–860.
- 26 N. Jost, K. Acsai, B. Horvath, T. Banyasz, I. Baczko, M. Bitay, et al., Contribution of I_{Kr} and I_{K1} to ventricular repolarization in canine and human myocytes: is there any influence of action potential duration? *Basic Res. Cardiol.* 104 (2009) 33–41.
- 27 B. Hegyi, B. Horváth, K. Vácz, M. Gönczi, K. Kistamas, F. Ruzsnavszky, et al., Ca^{2+} -activated Cl^- current is antiarrhythmic by reducing both spatial and temporal heterogeneity of cardiac repolarization, *J. Mol. Cell. Cardiol.* 109 (2017) 27–37.
- 28 T. Banyasz, L. Fulop, J. Magyar, N. Szentandrassy, A. Varro, P.P. Nanasi, Endocardial versus epicardial differences in L-type calcium current in canine ventricular myocytes studied by action potential voltage clamp, *Cardiovasc. Res.* 58 (2003) 66–75.
- 29 T. Bányász, J. Magyar, N. Szentandrassy, B. Horváth, P. Birinyi, J. Szentmiklósi, et al., Action potential clamp fingerprints of K^+ currents in canine cardiomyocytes: their role in ventricular repolarization, *Acta Physiol. Scand.* 190 (2007) 189–198.
- 30 T. Banyasz, B. Horvath, Z. Jian, L.T. Izu, C.-I. Ye, Profile of L-type Ca^{2+} current and Na^+ / Ca^{2+} exchange current during cardiac action potential in ventricular myocytes, *Heart Rhythm.* 9 (2012) 134–142.
- 31 B. Hegyi, B. Horváth, L. Bárándi, F. Papp, J. Magyar, T. Bányász, et al., Tetrodotoxin blocks L-type Ca^{2+} channels in canine ventricular cardiomyocytes, *Pflügers Arch.* 464 (2012) 167–174.
- 32 B. Hegyi, I. Komáromi, K. Kistamas, F. Ruzsnavszky, K. Vácz, B. Horváth, et al., Tetrodotoxin blockade on canine cardiac L-type Ca^{2+} channels depends on pH and redox potential, *Marine Drugs* 11 (2013) 2140–2153.

- [33] W.A. Catterall, Neurotoxins that act on voltage-sensitive sodium channels in excitable membranes, *Ann. Rev. Pharmacol. Toxicol.* 20 (1980) 15–43.
- [34] R. Bonatti, A.F. Silva, J.A. Batatinha, L.F. Sobrado, A.D. Machado, B.B. Varone, et al., Selective late sodium current blockade with GS-458967 markedly reduces ischemia-induced atrial and ventricular repolarization alternans and ECG heterogeneity, *Heart Rhythm*. 11 (2014) 1827–1835.
- [35] L. Belardinelli, G. Liu, C. Smith-Maxwell, W.Q. Wang, N. El-Bizri, R. Hirakawa, et al., A novel, potent, and selective inhibitor of cardiac late sodium current suppresses experimental arrhythmias, *J. Pharmacol. Exp. Ther.* 344 (2013) 23–32.
- [36] S. Jia, J. Lian, D. Guo, X. Xue, C. Patel, L. Yang, et al., Modulation of the late sodium current by ATX-II and ranolazine affects the reverse use-dependence and proarrhythmic liability of I_{Kr} blockade, *Br. J. Pharmacol.* 164 (2011) 308–316.
- [37] C.E. Clancy, M. Tateyama, H. Liu, X.H. Wehrens, R.S. Kass, Non-equilibrium gating in cardiac sodium channels: an original mechanism of arrhythmia, *Circulation* 107 (2003) 2233–2237.
- [38] M. Biet, H. Barajas-Martínez, A.T. Ton, J.F. Delabre, N. Morin, R. Dumaine, About half of the late sodium current in cardiac myocytes from dog ventricle is due to non-cardiac-type Na^+ channels, *J. Mol. Cell. Cardiol.* 53 (2012) 593–598.
- [39] W. Song, W. Shou, Cardiac sodium channel Nav 1.5 mutations and cardiac arrhythmia, *Pediatr. Cardiol.* 33 (2012) 943–949.
- [40] D.M. Roden, Long QT syndrome: reduced repolarization reserve and the genetic link, *J. Intern. Med.* 259 (2006) 59–69.
- [41] A. Varró, I. Baczkó, Cardiac ventricular repolarization reserve: a principle for understanding drug-related proarrhythmic risk, *Br. J. Pharmacol.* 164 (2011) 14–36.
- [42] N. Jost, L. Virág, P. Comtois, B. Ördög, V. Szuts, Seprényi Gy, et al., Ionic mechanisms limiting cardiac repolarization reserve in humans compared to dogs, *J. Physiol.* 591 (2013) 4189–4206.
- [43] S. Zicha, I. Moss, B. Allen, A. Varro, J. Papp, R. Dumaine, et al., Molecular basis of species-specific expression of repolarizing K^+ currents in the heart, *Am. J. Physiol. Heart Circ. Physiol.* 285 (2003) H1641–H1649.